LANGMUIR Article
Cite This: Langmuir 2019, 35, 4117−4124 pubs.acs.org/Langmuir

Ion-Induced Formation of Nanocrystalline Cellulose Colloidal Glasses Containing Nematic Domains

Pascal Bertsch,*[,†] Antoni Sánchez-Ferrer,[†] Massimo Bagnani,[†] Stéphane Isabettini,[†] Joachim Kohlbrecher,[‡] Raffaele Mezzenga,[†] and Peter Fischer*[,†]

[†]Institute of Food Nutrition and Health, ETH Zurich, 8092 Zurich, Switzerland
[‡]Laboratory for Neutron Scattering and Imaging, Paul Scherrer Institute, PSI, 5232 Villigen PSI, Switzerland

Supporting Information

ABSTRACT: Controlling the assembly of colloids in dispersion is a fundamental approach toward the production of functional materials. Nanocrystalline cellulose (NCC) is a charged nanoparticle whose colloidal interactions can be modulated from repulsive to attractive by increasing ionic strength. Here, we combine polarized optical microscopy, rheology, and small-angle scattering techniques to investigate (i) the concentration-driven transition from isotropic dispersion to cholesteric liquid crystals and (ii) salt-induced NCC phase transitions. In particular, we report on the formation of NCC attractive glasses containing nematic domains. At increasing NCC concentration, a structure peak was observed in small-angle X-ray scattering (SAXS) patterns. The evolution of the structure peak demonstrates the decrease in NCC interparticle distance, favoring orientational order during the isotropic−cholesteric phase transition. Small amounts of salt reduce the cholesteric volume fraction and pitch by a decrease in excluded volume. Beyond a critical salt concentration, NCC forms attractive glasses due to particle caging and reduced motility. This results in a sharp increase in viscosity and formation of viscoelastic glasses. The presence of nematic domains is suggested by the appearance of interference colors and the Cox−Merz rule failure and was confirmed by an anisotropic SAXS scattering pattern at q ranges associated with the presence of nematic domains. Thus, salt addition allows the formation of NCC attractive glasses with mechanical properties similar to those of gels while remaining optically active owed to entrapped nematic domains.

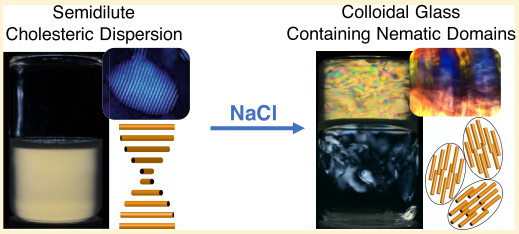

INTRODUCTION

Nanocrystalline cellulose (NCC) is a nanoparticle of biological origin readily exploited for its cholesteric self-assembly, allowing the formation of materials with desired structural and optical properties.[1,2] Its anisotropic shape and surface charge favor phase separation into an isotropic and a chiral nematic (or cholesteric) phase beyond a critical volume fraction ϕ_c.[3−6] The NCC employed here was gained from wood pulp by sulfuric acid hydrolysis, yielding anisotropic nanocrystals with an aspect ratio of ≈16 and charged sulfate ester residues.[7] Small amounts of salt (<3 mM NaCl) increase ϕ_c by decreasing the excluded volume, as predicted by Onsager's theory[8] and shown experimentally.[9−12] At high salt concentrations (>30 mM NaCl), attractive forces within NCC dominate, associated with the formation of viscoelastic hydrogels.[13−16]

Although NCC cholesteric phases and hydrogels have been studied intensively, NCC phase behavior at intermediate salt concentrations (4−30 mM NaCl) is not fully resolved. Upon salt-induced charge screening, the NCC crystallites arrest at a smaller interparticle distance and are caged by the potential setup of neighboring particles.[17,18] Due to a significant decrease in particle mobility, such systems are referred to as attractive glasses.[19,20] Further, there is evidence for the formation of nematic domains within NCC attractive glasses.[16,21,22] The angular dependence of electrostatic particle interactions and resulting twist vanishes at this ionic strength, promoting a nematic arrangement with infinite twist.[23,24] Similar observations were reported for other charged, anisotropic particles, like viruses,[18,25] proteins,[26,27] and inorganic particles.[17,28] Such salt-induced NCC glasses could be of interest as they exhibit mechanical properties similar to those of gels, keeping the optical activity known from liquid crystals.[16,17]

We demonstrate the salt-induced transition from semidilute cholesteric dispersions to colloidal glasses for charged anisotropic NCC. The optical and mechanical transitions were assessed and the underlying structural changes were determined using small-angle X-ray scattering (SAXS). This allows the formation of viscoelastic, optically active glasses with a broad range of potential applications.

MATERIALS AND METHODS

Materials. Milli-Q water was obtained from a Merck Millipore system (Darmstadt, Germany) and D_2O (99.9 atom % D) from ARMAR Chemicals (Döttingen, Switzerland). NaCl was purchased from Thermo Fisher (Zug, Switzerland).

Received: January 29, 2019
Revised: February 23, 2019
Published: February 27, 2019

DOI: 10.1021/acs.langmuir.9b00281
Langmuir 2019, 35, 4117−4124

NCC Characterization. NCC was kindly provided by CelluForce (Montreal, Canada). The NCC crystallites are 79 ± 6 nm in length and 4.75 ± 0.05 nm in height, as determined by atomic force microscopy.[7] No counterion condensation is expected at the linear charge density of 0.67 nm^{-1} (0.33 mmol/g, determined titrimetrically by the SCAN-CM 65:02 protocol).[16] The native-ion content was determined by atomic absorption spectroscopy and is negligible compared with salt concentrations added.[16] The critical volume fraction ϕ_c was approximated from an adaptation of Onsager's approach that accounts for the charged double layer of NCC.[29] The detailed calculations are provided in the Supporting Information.

NCC Dispersion Preparation. NCC was dispersed in Milli-Q water under stirring and the dispersions sonicated with a Hielscher UP200S (Teltow, Germany) at 160 W to a total energy input of 5000 J/g NCC to provide full dispersion.[30] Salts were added as 1 M solution and the sonication repeated to prevent salt-induced aggregates.

Polarized Optical Microscopy (POM). Polarized optical microscopy (POM) was performed in transmission mode on a Leica DMC 4500 light microscope (Heerbrugg, Switzerland). Samples were loaded in homemade cuvettes with a thickness of 100 μm. Two microscope slides were glued with a two-component glue using a 100 μm thick commercial tape as separator. The NCC dispersions were loaded and the capillaries sealed using the two-component glue. The chiral nematic pitch was determined from 20 tactoids using Image J.

Polarized Light Photography. Samples were loaded in 25 mL Wheaton flasks L6225 (Wheaton) for 10 days. The flasks were turned upside down and kept for another 10 days. The samples were photographed with a Nikon D800E equipped with a Nikon 55 mm macro lens (Tokyo, Japan) between cross-polarizers with a light source behind the samples.

Rheological Analysis. Rheological experiments were performed on a Physica MCR 702 rheometer (Anton Paar, Graz, Austria) equipped with a Couette CC27 geometry. A time sweep was performed directly after sonication at an angular frequency ω of 1 rad/s and strain γ of 0.5%. After 24 h, a frequency sweep and flow curve experiment were performed from 0.1−100 rad/s and 1/s, respectively, to evaluate structure build-up by application of the Cox−Merz rule.[31] Experiments were performed at 25 °C and samples covered by an medium chain triglyceride oil film.

ζ-Potential Measurements. The ζ-potential was determined with a Malvern Zetasizer nano ZS (Malvern, U.K.). A 0.1 wt % NCC dispersion was analyzed at pH 7 and 25 °C.

Small- and Wide-Angle X-ray Scattering (WAXS). Small- and wide-angle X-ray scattering (SAXS and WAXS) experiments were performed using Rigaku MicroMax-002+ (Tokyo, Japan) equipped with a microfocused beam (40 W, 45 kV, 0.88 mA) with the $\lambda_{Cu\ K\alpha}$ = 0.15418 nm radiation collimated by three pinhole collimators (0.4, 0.3, and 0.8 mm). Samples were loaded in 2 mm quartz capillaries and aligned in the X-ray beam. The SAXS and WAXS intensities were collected by a two-dimensional (2D) Triton-200 gas-filled X-ray detector (20 cm diameter, 200 μm resolution) and a two-dimensional Fujifilm BAS-MS 2025 (Tokyo, Japan) imaging plate system (15.2 × 15.2 cm^2, 50 μm resolution), respectively. An effective scattering vector range of 0.05 $nm^{-1} < q < 25\ nm^{-1}$ was obtained, where q is the scattering wave vector defined as $q = 4\pi \sin(\theta)/\lambda_{Cu\ K\alpha}$ with a scattering angle of 2θ.

RESULTS AND DISCUSSION

Self-Assembly and Salt-Induced Phase Transitions in NCC Dispersions. The critical volume fraction ϕ_c for the isotropic−cholesteric phase transition of NCC can be approximated by an adaptation of Onsager's hard-core repulsive model that accounts for the effective diameter D_{eff} of charged particles, $\phi_c = 3.34D^2/D_{eff}L$,[29] where D and L are the width and length of NCC, respectively. The D_{eff} of NCC was approximated to 27.4 nm (for details, see the Supporting Information). This results in ϕ_c = 0.035 or 5.1 wt % (assuming NCC density = 1.5 g/cm^3). This is a slight overestimation compared to experimental approaches that report 3−4 wt % depending on NCC dimensions and charge density.[21,32,33] This discrepancy probably derives from the polydispersity of NCC.

NCC colloidal behavior and self-assembly are determined by its charged double layer and ultimately the presence of counterions. Figure 1A visualizes the transitions of a 5 wt %

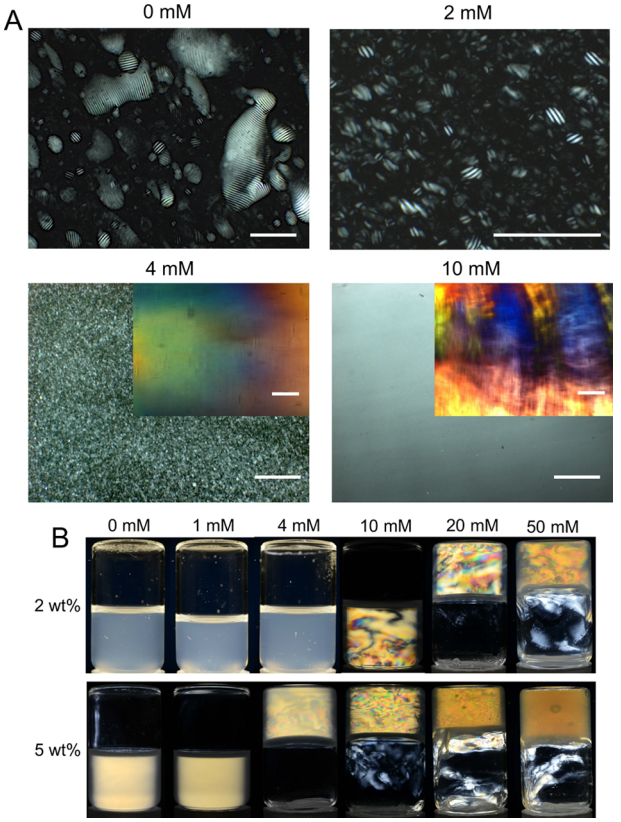

Figure 1. NCC dispersions (5 wt %) at increasing NaCl concentration visualized by (A) polarized optical microscopy images of NCC dispersion loaded in 100 μm cuvettes. The insets correspond to a sample thickness of 2 mm, demonstrating the onset of interference colors. The scale bar corresponds to 100 μm. (B) Macroscopic appearance of NCC dispersions placed between cross-polarizers.

NCC dispersion upon NaCl addition using POM. Without additional salt, cholesteric tactoids with a characteristic pitch of 9.75 ± 0.52 μm were observed, confirming that 5 wt % > ϕ_c and the respective dispersions are in the biphasic regime. NCC tactoids were recently demonstrated to be left-handed.[5] At 2 mM NaCl, the tactoids decreased in size (note the different scale bar) and the pitch decreased to 7.87 ± 0.54 μm. Salt concentrations from 0 to 2 mM are known to decrease the pitch and increase ϕ_c, associated with a lower cholesteric volume fraction.[9−12] This is attributed to the salt-induced charge screening and decrease in D_{eff}. The approximated D_{eff} at 2 mM is 15.8 nm, resulting in ϕ_c = 0.061 or 8.8 wt %. This is again an overestimation, although underlines the effect of salt on D_{eff} and ϕ_c numerically.

At 4 mM NaCl, no more tactoids were apparent. Beyond 4 mM NaCl, NCC dispersions form an attractive glass attributed to particle caging upon charge screening.[17,18] The samples

DOI: 10.1021/acs.langmuir.9b00281
Langmuir 2019, 35, 4117−4124

showed no reflection of left-handed circularly polarized light (not shown), demonstrating the absence of left-handed chiral nematic domains. However, there is evidence that NCC attractive glasses may contain nematic domains.[16,21,22] This is associated with a colorful appearance beyond a critical sample thickness, as demonstrated by the insets taken from 2 mm quartz cuvettes. This indicates that the colors derive from the optical phase retardation of light passing through an anisotropic material, also known as interference colors.[34]

The same transitions were apparent for macroscopic NCC dispersions (Figure 1B). NCC (5 wt %) dispersions display birefringence under cross-polarizers. From 4 mM NaCl, 5 wt % NCC dispersions formed attractive glasses that resist gravity and exhibit interference colors, in agreement with POM. Such volume spanning attractive glasses may be formed at NCC concentrations as low as 2 wt %, although 10 mM NaCl is required. This is in contrast to approximately 10 wt % required to form volume-spanning chiral nematic phases from NCC.[21,32,33] At 50 mM NaCl, attractive van der Waals and hydrophobic forces dominate, inducing the formation of translucent hydrogels. This demonstrates the transition from NCC attractive glasses to hydrogels upon full charge screening and NCC aggregation. Interestingly, 2 wt % NCC dispersions still showed interference colors at 50 mM, suggesting that at low particle concentrations full NCC aggregation is not possible.

The influence of small amounts of salt on NCC chiral nematic ordering[9−12] and ion-induced NCC hydrogels[13−16] are well established in literature. Comparably little is known about NCC attractive glasses and the formation of nematic domains therein. NCC attractive glasses may be formed by increasing ionic strength[16,21,22] or decreasing NCC charge density.[20] Note the difference to repulsive glasses, which may be formed by an increase in NCC concentration.[19,20] Attractive glasses are characterized by an interplay of repulsive and attractive interactions, resulting in particle caging and low motility. As demonstrated above using polarized light, nematic domains are formed in NCC attractive glasses. Some sources report a steady decrease in pitch upon salt addition, in line with our findings, followed by an increase around 2 mM NaCl.[12,22] This may indicate the continuous second-order transition from a chiral nematic to a nematic phase with infinite pitch. This is in agreement with theory, that predicts a decrease of the angular dependence of electrostatic interactions and the resulting twist at increasing ionic strength.[23,24] Thus, the mobility constraints in attractive glasses seem to favor the formation of nematic domains. An ordered structural arrest upon salt addition was also observed for other charged anisotropic particles such as viruses,[18,25] proteins,[26,27] and inorganic particles.[17,28]

NCC shows great potential in the production of optical materials, as its visual appearance may be controlled by the underlying structure.[2] Such materials are commonly produced by drying chiral nematic phases into thin films. NCC attractive glasses containing nematic domains may provide a new approach toward the production of NCC optical materials. It was previously suggested by Gençer et al.[35] that salt addition modulates the structural and optical properties of NCC thin films.

In this work, we employ NaCl to demonstrate salt-induced phase transitions in NCC dispersions. However, as the driving force is decreasing electrostatic repulsion, the same phase transitions may be induced by other salts,[15,16] although lower concentrations of divalent or trivalent salts are required due to more efficient charge screening. This is demonstrated for $CaCl_2$ in Figure S1.

Detecting Salt-Induced Phase Transitions Using Rheology. Rheology was amongst the first methods used to study the formation of attractive glasses.[17] The salt-induced charge screening is related to an increase in dispersion viscosity, which allows to determine NCC colloidal behavior and phase transitions.[13,16] Figure 2A presents the equilibrium complex viscosity η^* of NCC dispersions as a function of NaCl concentration. The inset shows the respective ζ-potential, the magnitude of electrostatic repulsion within NCC crystallites as a function of NaCl concentration. The evolution of η^* as a function of NaCl concentration is in good agreement with visually observed NCC phase behavior. At 1 mM NaCl, η^* decreased due a decrease in D_{eff}. This is known as the electroviscous effect and commonly observed for NCC.[16,36] Hence, NCC electrostatic repulsion is still predominant. The formation of attractive glass at ≈4 mM NaCl was associated with a sharp increase in η^*. The increased viscosity was recently shown to be beneficial for NCC film drying, as it prevents coffee ring formation and results in more uniform films.[35] Above 30 mM NaCl, attractive forces dominate and NCC forms hydrogels approaching a maximum η^*. For clarity, further data are presented in the following color code. Blue: dominating electrostatic repulsion (cholesteric). Orange: equilibrium (attractive glass). Green: dominating attractive forces (hydrogel).

The attractive glasses showed a distinctive increase in η^* over several hours, as shown in Figure 2B. Similar arresting dynamics were observed by Xu et al.[13] at this salt concentration. In contrast, minor changes occurred for cholesteric samples. The hydrogels attained equilibrium η^* after 1 h, in line with NCC gelation kinetics determined by light scattering.[37] Figure 2C depicts dynamic frequency sweeps performed after 24 h of equilibration, illustrating the transition from liquidlike NCC dispersions ($G' < G''$) without salt to an increasingly elastic response upon salt addition. The transition ($G' = G''$) occurred at 5 mM, in good agreement with the glass transition. Ten milimolar samples showed a gel-like response ($G' > G''$) with frequency-independent dynamic moduli. The macroscopic samples were previously demonstrated to resist gravity from above 4 mM NaCl (see Figure 1).

Finally, the presence of nematic domains was confirmed by application of the Cox−Merz rule,[31] stating that η^* and shear viscosity η match for isotropic but diverge for structured fluids. Figure 2D depicts η^* (full) and η (empty) as a function of the frequency and shear rate, respectively. At low salt concentrations, η^* and η were equal and thus followed the Cox−Merz rule. At higher salinity, η^* and η increasingly deviated, indicating the presence of anisotropic nematic domains. Under shear, the ordered domains are broken, resulting in constant η at increasing salt concentration. On the other hand, η^* increases with salinity. This supports the presence of nematic domains in NCC attractive glasses, although it is not entirely clear if the Cox−Merz rule failure generally arises in colloidal glasses. The Cox−Merz rule failure of hydrogels at high salt concentrations can be attributed to the weak aggregation of NCC upon charge screening, which is reversible upon shear.[13,20]

After shear, NCC glasses and hydrogels rebuild according to the kinetics shown in Figure 2B. This fully reversible shear-thinning behavior qualifies NCC attractive glasses for three-

DOI: 10.1021/acs.langmuir.9b00281
Langmuir 2019, 35, 4117−4124

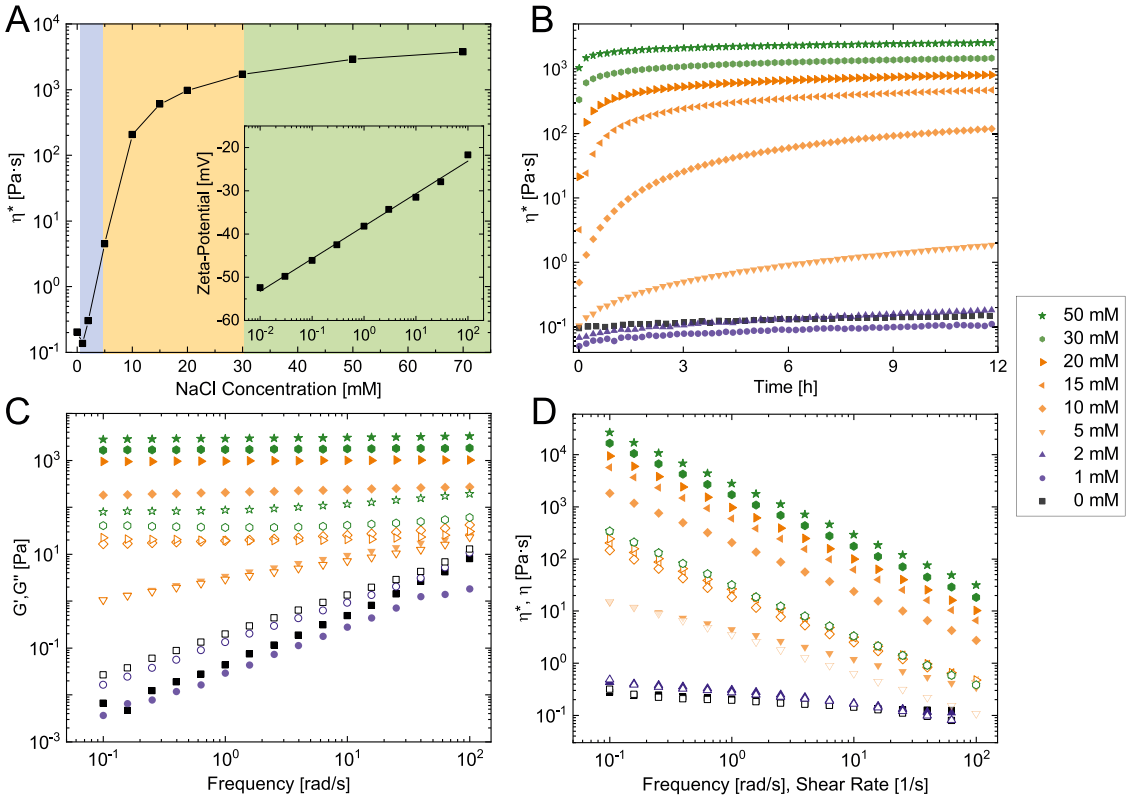

Figure 2. Rheological analysis of 5 wt % NCC dispersions at increasing NaCl concentration. (A) Complex viscosity η^* as a function of NaCl concentration after 24 h. The line is to guide the eye. The inset depicts the corresponding ζ-potential of a 0.1 wt % NCC dispersion as a function of NaCl concentration. (B) η^* as a function of time after sonication. (C) Dynamic storage (G', full) and loss (G'', empty) moduli as a function of angular frequency after 24 h. (D) Cox–Merz rule comparison showing η^* (full) and shear viscosity η (empty) as a function of angular frequency and shear rate, respectively. Oscillatory experiments were performed at ω = 1 rad/s and γ = 0.5%. The temperature was set to 25 °C.

dimensional (3D) printing or biomedical injections.[38,39] This could allow to exploit the structural or optical anisotropy of NCC in these applications. NCC was previously used to print hierarchical structures with desired mechanical[38] or optical[40] properties. Further, the salt-induced increase in viscosity could enable these applications at reduced NCC concentrations. To achieve similar η^* or G' without salt addition, NCC concentrations of ≈10 wt % NCC are required.[30,33]

Probing NCC Structure and Semidilute Ordering Using WAXS and SAXS. To understand the self-assembly and salt-induced phase transitions in NCC dispersions, detailed knowledge of NCC single crystallite structure is required. Figure 3A depicts the WAXS intensity profile of NCC powder. Five peaks representing crystalline structures (blue) were observed and could be attributed to individual crystal planes, as indicated in the graph. Comparison of the integrated area of crystalline and amorphous (green) peaks revealed that NCC crystallinity χ was 78%. The determined unit cell (a = 8.3 Å, b = 8.1 Å, c = 10.3 Å, γ = 95.8°) corresponds to a monoclinic (Iβ) structure consisting of two glucose chains, as common for celluloses from plant cell walls.[41,42] The radial width of a crystallite was approximated to 5 nm from the intensity of the xy crystal plane peaks. This is in line with 4.75 nm obtained from atomic force microscopy images[7] and corresponds to six unit cells. The axial domain size was approximated to 10 nm from the the q_{004} peak. This corresponds to the NCC correlation length and can be considered the axial subunit of NCC crystallites. Figure 3B shows WAXS intensity profiles of NCC in dispersion at different salt concentrations. The q_{020} crystal plane peak was still apparent in dispersion, confirming that no structural changes occur upon hydration.[43] The addition of 10 mM NaCl did not induce any changes in the WAXS pattern. This confirms that salt-induced phase transitions in NCC dispersions are derived entirely from charge screening and altering NCC interaction potential and no structural changes occur on the single crystallite level.

Figure 3C depicts SAXS intensity profiles for increasing NCC dispersion concentrations without salt. For NCC concentrations <0.5 wt %, the intensity profiles were well described by the form factor (extracted from the 0.02 wt % SAXS intensity profile). Thus, no NCC interactions occur at these concentrations and the crystallites can be assumed isotropically oriented. From 0.5 wt %, a structure factor $S(q)$ was obtained, indicating arising NCC interactions. Figure 3D shows $S(q)$ derived from a square well potential model (see Figure S2 for fits). The increasing NCC interaction potential was associated with a structure peak in the intensity profile $I(q)$ and corresponding $S(q)$. This peak correlates to the statistically prevalent interparticle distance d. The peak was shifted to higher q values at increasing NCC concentration, demonstrating closer NCC packing. The shift was proportional to $\sqrt{\phi}$, as expected for rigid rodlike particles.[44] Upcoming structure factor contributions associated with a change in slope at $q \approx 0.1$ nm^{-1} are consistent with previous small-angle scattering studies.[32,45−47] Uhlig et al.[47] attributed the structure peak to the formation of 2D aggregates, which was considered the onset of liquid-crystalline ordering. The extracted

DOI: 10.1021/acs.langmuir.9b00281
Langmuir 2019, 35, 4117−4124

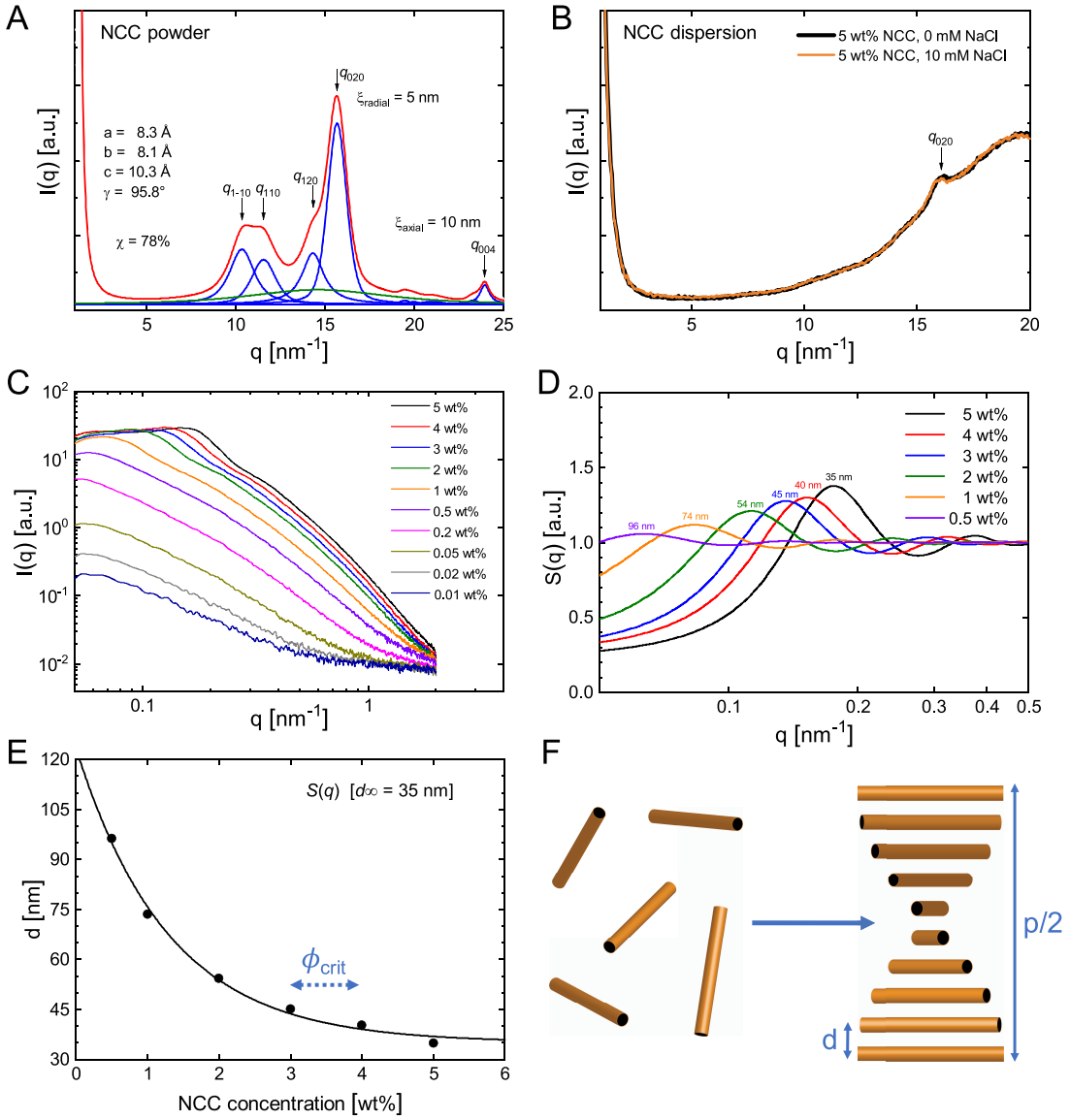

Figure 3. (A) One-dimensional WAXS intensity profile of NCC powder showing crystalline (blue) and amorphous (green) peaks. The corresponding crystal planes and unit cell parameters are indicated in the graph. (B) One-dimensional WAXS intensity profile of 5 wt % NCC dispersions at 0 and 10 mM NaCl. (C) One-dimensional SAXS intensity profiles of dispersions at increasing NCC concentration and (D) corresponding structure factors $S(q)$. (E) Extracted interparticle distance d as a function of NCC concentration. (F) Schematic transition from isotropic dispersion to a chiral nematic phase with characteristic interparticle distance d and pitch p.

interparticle distance d is plotted as a function of NCC concentration in Figure 3E. A statistically prevalent d in the range of 100 nm is already observed in the isotropic dispersion at 0.5 wt % NCC, way below ϕ_c. The particle distance d decays exponentially at increasing NCC concentration and is ≈50 nm at ϕ_c (3−4 wt %). This seems to be the critical distance at which particle interactions promote the formation of a cholesteric phase with orientational order. The transition from isotropic dispersion to a chiral nematic phase with periodical spacing d and pitch p is illustrated in Figure 3F. A minimum distance d_∞ = 35 nm was found, in good agreement with the approximated D_{eff} = 27.4 nm used above to calculate ϕ_c. As SAXS provides a statistical d, it cannot be conclusively attributed to either the distance within nematic planes or the distance of particles within the same nematic plane. For the first case, all tactoids would have to be perpendicularly oriented to the beam.[48] Assuming d_∞ = 35 nm as the distance within nematic planes and considering the pitch of 9.75 μm at 5 wt % NCC results in ≈279 crystallites with a twisting angle of 1.29° for a full 360° twist. Schütz et al.[32] found that d_∞ = 25 nm for NCC similar in size but with lower surface charge density (0.33 and 0.23 mmol/g, respectively). Thus, lower NCC charge density results in closer NCC packing, which ultimately affects the chiral nematic pitch. It is known that NCCs from different sources show differences in ϕ_c and pitch depending on their aspect ratio and charge density.[49]

As indicated above, a viscoelastic attractive glass containing nematic domains may be formed from such semidilute dispersions by targeted salt addition. The underlying structural changes are elaborated in the following section.

Structural Evolution During Salt-Induced Formation of NCC Attractive Glasses. Figure 4A depicts the evolution of SAXS intensity profiles of NCC dispersions at increasing NaCl concentration. A zoom-in of the relevant q range is

DOI: 10.1021/acs.langmuir.9b00281
Langmuir 2019, 35, 4117−4124

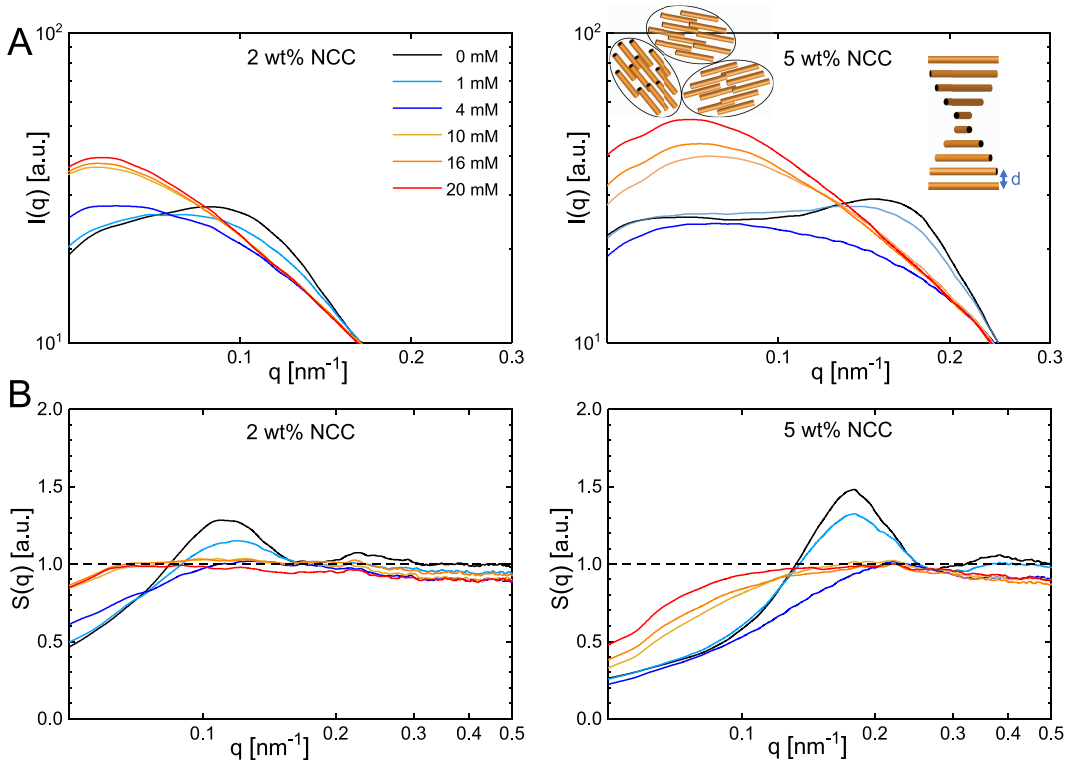

Figure 4. (A) One-dimensional SAXS intensity profiles and (B) corresponding structure factors $S(q)$ of 2 wt % (left) and 5 wt % (right) NCC dispersions at increasing NaCl concentration.

shown. The entire SAXS intensity profiles including further NaCl concentrations, as well as small-angle neutron scattering (SANS) intensity profiles upon adding $CaCl_2$ are provided as Figures S3 and S4. For NCC dispersions without added salt, the structure peak was apparent at $q \approx 0.11$ and 0.18 nm^{-1} for 2 and 5 wt % NCC, respectively. The peak intensity diminished at 1 mM and completely vanished at 4 mM NaCl. This demonstrates the effect of charge screening and decreased D_{eff} upon salt addition. This q range was also seen to be affected by salt addition at NCC concentrations below the appearance of structure peaks, allowing the determination of NCC interaction potential upon salt addition.[14,15,45] The structure peaks were observed at the same q values in SANS experiments and diminished upon $CaCl_2$ addition (Figure S4).

The formation of attractive glasses at 10 mM NaCl was associated with a sudden structural change. A new peak arose at lower q ranges of 0.057 and 0.073 nm^{-1} for 2 and 5 wt % NCC, respectively. An anisotropic scattering pattern at a lower q range compared to that of the structure peak is indeed expected for nematic domains.[50] This provides the structural proof for the formation of nematic domains within attractive NCC glasses. The critical NaCl concentration correlates with arising interference colors (Figure 1) and Cox–Merz rule failure (Figure 2D) attributed to the formation of nematic domains. Kang and Dhont[18] could previously link the salt-induced structural arrest of charged anisotropic rods to the formation of nematic domains with different orientations. Figure 4B shows the evolution of the structure factor upon salt addition. The peak, which corresponds to the secondary minimum according to the DLVO theory, decreases upon salt addition due to charge screening. No correlation peak was observed for salt-induced nematic domains, as expected for nematic phases with no positional order.

CONCLUSIONS

The charged nature of nanocrystalline cellulose (NCC) allows the transition from cholesteric liquid crystals to attractive glasses at increasing ionic strength. Here, we investigated the related optical and mechanical transitions and linked them to the underlying structural changes using small-angle scattering techniques.

The isotropic–nematic transition of NCC was investigated using small-angle X-ray scattering (SAXS). At increasing NCC concentration, the interparticle distance decreases until particle interactions promote the formation of a cholesteric phase with orientational order. Salt addition initially decreases the cholesteric volume fraction and pitch. From a critical concentration of 4 mM NaCl (or ≈2 mM divalent $CaCl_2$), NCC forms attractive glasses. This is attributed to particle caging and reduced motility and was associated with a sharp increase in viscosity. NCC attractive glasses revealed viscoelastic properties similar to those of hydrogels commonly formed at higher salt concentrations. Due to their shear-thinning behavior and recovery after shear, NCC attractive glasses qualify for 3D printing or biomedical injection.

NCC attractive glasses exhibited interference colors under cross-polarizers, suggesting the presence of nematic domains. This was supported rheologically by the Cox–Merz rule failure and ultimately confirmed using SAXS. Thus, salt addition allows the formation of viscoelastic glasses containing optically active nematic domains. Their optical and mechanical properties can be modulated by varying NCC and salt concentration. This could provide a new approach toward the production of NCC-based optical materials at increased structural flexibility.

DOI: 10.1021/acs.langmuir.9b00281
Langmuir 2019, 35, 4117–4124

■ ASSOCIATED CONTENT

Supporting Information

The Supporting Information is available free of charge on the ACS Publications website at DOI: 10.1021/acs.langmuir.9b00281.

Detailed calculation of D_{eff} and ϕ_c; macroscopic NCC dispersions between cross-polarizers with phase transitions induced using $CaCl_2$; SAXS structure factors fitted using square well potential fits; SAXS intensity profiles of NCC dispersions and added NaCl for the entire q range and further NaCl concentrations; SANS intensity profiles for NCC dispersions with added $CaCl_2$ (PDF)

■ AUTHOR INFORMATION

Corresponding Authors

*E-mail: pascal.bertsch@hest.ethz.ch. Phone: +41 44 632 67 62 (P.B.).

*E-mail: peter.fischer@hest.ethz.ch (P.F.).

ORCID

Pascal Bertsch: 0000-0002-9188-2912

Antoni Sánchez-Ferrer: 0000-0002-1041-0324

Massimo Bagnani: 0000-0002-1326-1600

Stéphane Isabettini: 0000-0003-3416-8103

Raffaele Mezzenga: 0000-0002-5739-2610

Peter Fischer: 0000-0002-2992-5037

Notes

The authors declare no competing financial interest.

■ ACKNOWLEDGMENTS

The authors acknowledge CelluForce for providing NCC and thank Mario Arcari and Lukas Böni for helpful discussions. SANS experiments were performed at the Swiss Spallation Neutron Source SINQ, Paul Scherrer Institute, Villigen PSI, Switzerland. This project was funded by the Swiss National Science Foundation, Project Nos. 200021-137941 and 200021-175994.

■ REFERENCES

(1) Shopsowitz, K. E.; Qi, H.; Hamad, W. Y.; MacLachlan, M. J. Free-Standing Mesoporous Silica Films with Tunable Chiral Nematic Structures. *Nature* **2010**, *468*, 422−425.

(2) Parker, R. M.; Guidetti, G.; Williams, C. A.; Zhao, T.; Narkevicius, A.; Vignolini, S.; Frka-Petesic, B. The Self-Assembly of Cellulose Nanocrystals: Hierarchical Design of Visual Appearance. *Adv. Mater.* **2018**, *30*, No. e1704477.

(3) Revol, J.-F.; Bradford, H.; Giasson, J.; Marchessault, R.; Gray, D. Helicoidal Self-Ordering of Cellulose Microfibrils in Aqueous Suspension. *Int. J. Biol. Macromol.* **1992**, *14*, 170−172.

(4) Gray, D. G. Order and Gelation of Cellulose Nanocrystal Suspensions: An Overview of Some Issues. *Philos. Trans. R. Soc., A* **2018**, *376*, No. 20170038.

(5) Nyström, G.; Arcari, M.; Adamcik, J.; Usov, I.; Mezzenga, R. Nanocellulose Fragmentation Mechanisms and Inversion of Chirality from the Single Particle to the Cholesteric Phase. *ACS Nano* **2018**, *12*, 5141−5148.

(6) Liu, Y.; Schütz, C.; Salazar-Alvarez, G.; Bergström, L. Assembly, Gelation and Helicoidal Consolidation of Nanocellulose Dispersions. *Langmuir* **2019**, DOI: 10.1021/acs.langmuir.8b04013.

(7) Bertsch, P.; Diener, M.; Adamcik, J.; Scheuble, N.; Geue, T.; Mezzenga, R.; Fischer, P. Adsorption and Interfacial Layer Structure of Unmodified Nanocrystalline Cellulose at Air/Water Interfaces. *Langmuir* **2018**, *34*, 15195−15202.

(8) Onsager, L. The Effects of Shape on the Interactions of Colloidal Paticles. *Ann. N. Y. Acad. Sci.* **1949**, *51*, 627−659.

(9) Dong, X. M.; Kimura, T.; Gray, D. G.; Revol, J.-F. Effects of Ionic Strength on the Isotropic - Chiral Nematic Phase Transition of Suspensions of Cellulose Crystallites. *Langmuir* **1996**, *12*, 2076−2082.

(10) Dong, X. M.; Gray, D. G. Effect of Counterions on Ordered Phase Formation in Suspensions of Charged Rodlike Cellulose Crystallites. *Langmuir* **1997**, *13*, 2404−2409.

(11) Pan, J.; Hamad, W.; Straus, S. K. Parameters Affecting the Chiral Nematic Phase of Nanocrystalline Cellulose Films. *Macromolecules* **2010**, *43*, 3851−3858.

(12) Honorato-Rios, C.; Kuhnhold, A.; Bruckner, J. R.; Dannert, R.; Schilling, T.; Lagerwall, J. P. F. Equilibrium Liquid Crystal Phase Diagrams and Detection of Kinetic Arrest in Cellulose Nanocrystal Suspensions. *Front. Mater.* **2016**, *3*, No. 21.

(13) Xu, Y.; Atrens, A. D.; Stokes, J. R. "Liquid, Gel and Soft Glass" Phase Transitions and Rheology of Nanocrystalline Cellulose Suspensions as a Function of Concentration and Salinity. *Soft Matter* **2018**, *14*, 1953−1963.

(14) Cherhal, F.; Cousin, F.; Capron, I. Influence of Charge Density and Ionic Strength on the Aggregation Process of Cellulose Nanocrystals in Aqueous Suspension, as Revealed by Small-Angle Neutron Scattering. *Langmuir* **2015**, *31*, 5596−5602.

(15) Phan-Xuan, T.; Thuresson, A.; Skepö, M.; Labrador, A.; Bordes, R.; Matic, A. Aggregation Behavior of Aqueous Cellulose Nanocrystals: The Effect of Inorganic Salts. *Cellulose* **2016**, *23*, 3653−3663.

(16) Bertsch, P.; Isabettini, S.; Fischer, P. Ion-Induced Hydrogel Formation and Nematic Ordering of Nanocrystalline Cellulose Suspensions. *Biomacromolecules* **2017**, *18*, 4060−4066.

(17) Wierenga, A.; Philipse, A. P.; Lekkerkerker, H. N. W.; Boger, D. V. Aqueous Dispersions of Colloidal Boehmite: Structure, Dynamics, and Yield Stress of Rod Gels. *Langmuir* **1998**, *14*, 55−65.

(18) Kang, K.; Dhont, J. K. G. Structural Arrest and Texture Dynamics in Suspensions of Charged Colloidal Rods. *Soft Matter* **2013**, *9*, 4401.

(19) Tanaka, H.; Meunier, J.; Bonn, D. Nonergodic States of Charged Colloidal Suspensions: Repulsive and Attractive Glasses and Gels. *Phys. Rev. E* **2004**, *69*, No. 031404.

(20) Nordenström, M.; Fall, A.; Nyström, G.; Wågberg, L. Formation of Colloidal Nanocellulose Glasses and Gels. *Langmuir* **2017**, *33*, 9772−9780.

(21) Honorato-Rios, C.; Lehr, C.; Schütz, C.; Sanctuary, R.; Osipov, M. A.; Baller, J.; Lagerwall, J. P. F. Fractionation of Cellulose Nanocrystals: Enhancing Liquid Crystal Ordering without Promoting Gelation. *NPG Asia Mater.* **2018**, *10*, 455−465.

(22) Hirai, A.; Inui, O.; Horii, F.; Tsuji, M. Phase Separation Behavior in Aqueous Suspensions of Bacterial Cellulose Nanocrystals Prepared by Sulfuric Acid Treatment. *Langmuir* **2009**, *25*, 497−502.

(23) Stroobants, A.; Lekkerkerker, H. N. W.; Odijk, T. Effect of Electrostatic Interaction on the Liquid Crystal Phase Transition in Solutions of Rodlike Polyelectrolytes. *Macromolecules* **1986**, *19*, 2232−2238.

(24) Fraden, S.; Maret, G.; Caspar, D. L. D.; Meyer, R. B. Isotropic-Nematic Phase Transition and Angular Correlations in Isotropic Suspensions of Tobacco Mosaic Virus. *Phys. Rev. Lett.* **1989**, *63*, No. 2068.

(25) Tang, J. X.; Wong, S.; Tran, P. T.; Janmey, P. A. Counterion Induced Bundle Formation of Rodlike Polyelectrolytes. *Ber. Bunsen-Ges. Phys. Chem.* **1996**, *100*, 796−806.

(26) Tang, J. X.; Ito, T.; Tao, T.; Traub, P.; Janmey, P. A. Opposite Effects of Electrostatics and Steric Exclusion on Bundle Formation by F-Actin and Other Filamentous Polyelectrolytes. *Biochemistry* **1997**, *36*, 12600−12607.

(27) Needleman, D. J.; Ojeda-Lopez, M. A.; Raviv, U.; Miller, H. P.; Wilson, L.; Safinya, C. R. Higher-Order Assembly of Microtubules by Counterions: From Hexagonal Bundles to Living Necklaces. *Proc. Natl. Acad. Sci. U.S.A.* **2004**, *101*, 16099−16103.

(28) Pelletier, O.; Davidson, P.; Bourgaux, C.; Livage, J. The Effect of Attractive Interactions on the Nematic Order of V_2O_5 Gels. *Europhys. Lett.* **1999**, *48*, 53−59.
(29) Mezzenga, R.; Jung, J.-M.; Adamcik, J. Effects of Charge Double Layer and Colloidal Aggregation on the Isotropic-Nematic Transition of Protein Fibers in Water. *Langmuir* **2010**, *26*, 10401−10405.
(30) Shafiei-Sabet, S.; Hamad, W. Y.; Hatzikiriakos, S. G. Rheology of Nanocrystalline Cellulose Aqueous Suspensions. *Langmuir* **2012**, *28*, 17124−17133.
(31) Cox, W. P.; Merz, E. H. Correlation of Dynamic and Steady Flow Viscosities. *J. Polym. Sci.* **1958**, *28*, 619−622.
(32) Schütz, C.; Agthe, M.; Fall, A. B.; Gordeyeva, K.; Guccini, V.; Salajková, M.; Plivelic, T. S.; Lagerwall, J. P. F.; Salazar-Alvarez, G.; Bergström, L. Rod Packing in Chiral Nematic Cellulose Nanocrystal Dispersions Studied by Small-Angle X-ray Scattering and Laser Diffraction. *Langmuir* **2015**, *31*, 6507−6513.
(33) Ureña-Benavides, E. E.; Ao, G.; Davis, V. A.; Kitchens, C. L. Rheology and Phase Behavior of Lyotropic Cellulose Nanocrystal Suspensions. *Macromolecules* **2011**, *44*, 8990−8998.
(34) Wu, S.-T.; Efron, U.; Hess, L. D. Birefringence Measurements of Liquid Crystals. *Appl. Opt.* **1984**, *23*, 3911−3915.
(35) Gençer, A.; Van Rie, J.; Lombardo, S.; Kang, K.; Thielemans, W. Effect of Gelation on the Colloidal Deposition of Cellulose Nanocrystal Films. *Biomacromolecules* **2018**, *19*, 3233−3243.
(36) Shafiei-Sabet, S.; Hamad, W. Y.; Hatzikiriakos, S. G. Ionic Strength Effects on the Microstructure and Shear Rheology of Cellulose Nanocrystal Suspensions. *Cellulose* **2014**, *21*, 3347−3359.
(37) Peddireddy, K. R.; Capron, I.; Nicolai, T.; Benyahia, L. Gelation Kinetics and Network Structure of Cellulose Nanocrystals in Aqueous Solution. *Biomacromolecules* **2016**, *17*, 3298−3304.
(38) Siqueira, G.; Kokkinis, D.; Libanori, R.; Hausmann, M. K.; Gladman, A. S.; Neels, A.; Tingaut, P.; Zimmermann, T.; Lewis, J. A.; Studart, A. R. Cellulose Nanocrystal Inks for 3D Printing of Textured Cellular Architectures. *Adv. Funct. Mater.* **2017**, *27*, No. 1604619.
(39) Guvendiren, M.; Lu, H. D.; Burdick, J. A. Shear-Thinning Hydrogels for Biomedical Applications. *Soft Matter* **2012**, *8*, 260−272.
(40) Zhao, T. H.; Parker, R. M.; Williams, C. A.; Lim, K. T. P.; Frka-Petesic, B.; Vignolini, S. Printing of Responsive Photonic Cellulose Nanocrystal Microfilm Arrays. *Adv. Funct. Mater.* **2018**, No. 1804531.
(41) Habibi, Y.; Lucia, L. A.; Rojas, O. J. Cellulose Nanocrystals: Chemistry, Aelf-Assembly, and Applications. *Chem. Rev.* **2010**, *110*, 3479−3500.
(42) Moon, R. J.; Martini, A.; Nairn, J.; Simonsen, J.; Youngblood, J. Cellulose Nanomaterials Review: Structure, Properties and Nanocomposites. *Chem. Soc. Rev.* **2011**, *40*, 3941.
(43) Maurer, R. J.; Sax, A. F.; Ribitsch, V. Molecular Simulation of Surface Reorganization and Wetting in Crystalline Cellulose I and II. *Cellulose* **2013**, *20*, 25−42.
(44) Kratky, O. X-Ray Small Angle Scattering with Substances of Biological Interest in Diluted Solutions. *Prog. Biophys. Mol. Biol.* **1963**, *13*, 105−173.
(45) Schmitt, J.; Calabrese, V.; da Silva, M. A.; Lindhoud, S.; Alfredsson, V.; Scott, J. L.; Edler, K. J. TEMPO-Oxidised Cellulose Nanofibrils; Probing the Mechanisms of Gelation via Small Angle X-ray Scattering. *Phys. Chem. Chem. Phys.* **2018**, *20*, 16012−16020.
(46) Orts, W. J.; Godbout, L.; Marchessault, R. H.; Revol, J.-F. Enhanced Ordering of Liquid Crystalline Suspensions of Cellulose Microfibrils: A Small Angle Neutron Scattering Study. *Macromolecules* **1998**, *31*, 5717−5725.
(47) Uhlig, M.; Fall, A.; Wellert, S.; Lehmann, M.; Prévost, S.; Wågberg, L.; von Klitzing, R.; Nyström, G. Two-Dimensional Aggregation and Semidilute Ordering in Cellulose Nanocrystals. *Langmuir* **2016**, *32*, 442−450.
(48) Klockars, K. W.; Tardy, B. L.; Borghei, M.; Tripathi, A.; Greca, L. G.; Rojas, O. J. Effect of Anisotropy of Cellulose Nanocrystal Suspensions on Stratification, Domain Structure Formation, and Structural Colors. *Biomacromolecules* **2018**, *19*, 2931−2943.
(49) Schütz, C.; Van Rie, J.; Eyley, S.; Gençer, A.; Van Gorp, H.; Rosenfeldt, S.; Kang, K.; Thielemans, W. Effect of Source on the Properties and Behavior of Cellulose Nanocrystal Suspensions. *ACS Sustainable Chem. Eng.* **2018**, *6*, 8317−8324.
(50) Pelletier, O.; Bourgaux, C.; Diat, O.; Davidson, P.; Livage, J. A Small-Angle X-Ray Scattering Study of the Isotropic and Nematic Phases of V_2O_5 Suspensions. *Eur. Phys. J. E* **2000**, *2*, 191−198.

DOI: 10.1021/acs.langmuir.9b00281
Langmuir 2019, 35, 4117−4124